www.ietdl.org

Published in IET Microwaves, Antennas & Propagation
Received on 21st July 2013
Revised on 11th January 2014
Accepted on 3rd June 2014
doi: 10.1049/iet-map.2013.0379

ISSN 1751-8725

Design and characterisation model for a linearly polarised patch array fed by serial rectangular waveguide network

Sergio Casas-Olmedo, Jose Luis Masa-Campos, Pablo Sánchez-Olivares

Department of Electronic and Communication Technologies, Group of Radio-Frequency, Circuits, Antennas and Systems (RFCAS), Autonoma University of Madrid, Francisco Tomas y Valiente 11, 28049 Madrid, Spain
E-mail: joseluis.masa@uam.es

Abstract: A novel method for considering radiating structures independently to their feeding networks is presented. The integration of both parts separately designed suffers a critical misalignment with the theoretical behaviour caused by the mutual coupling effects between adjacent elements. This method analyses radiated near E-field monitors to adjust the whole antenna after joining both independently designed parts. A linearly polarised patch array fed by a rectangular waveguide with internal coupling patches for X band (11–12 GHz) has been designed to validate the method performance. A double stacked microstrip patch structure with an integrated phase compensation microstrip line has been used as radiating element. The coupling patches inside the waveguide are connected to the external radiating patches by means of metallic probes. The presented method requires changes in the feeding structure as in the radiating elements. Several prototypes have been manufactured and measured: the feeding waveguide structure connectorised, the radiating patches connectorised, the union of both with SMA transitions and the final integration into the complete antenna. 18.5 dBi gain and 85% efficiency peak values, as well as 6% usable bandwidth have been experimentally achieved.

1 Introduction

During the last decades, in high frequency applications slots have been commonly used as radiating elements in waveguide arrays with satisfactory results in the whole microwave band [1–6]. However, these slotted waveguides lack in versatility because of the strong dependency between the radiating element and the feeding network. As an alternative, a design with patches instead of slots as single radiator was proposed by authors in [7]. In this case, a clear independency between both the feeding and radiating networks in the design process is then achieved. Also a new coupling structure between the wave propagated inside the waveguide and the external radiating patches was introduced, which is formed by internal coupling patches (ICPs) inside the waveguide. Exclusively for circularly polarised (CP) arrays, a technique to tune the radiated phase of each element consisting on the axial rotation of pin-fed elements as helixes [8], curls [9] and patches [10, 11]. Otherwise for linear polarisation (LP), the new coupling method provides the capacity of antenna reconfigurability by the insertion of structures ([12]) and devices ([13–15]) externally placed to the waveguide network to achieve a radiation pattern control. Finally in both [7, 12], the elements were individually designed with a basic cell model, without taking into account the degradation caused by the coupling effects between adjacent elements. These structures were fed by parallel plate waveguides. In [16], a substrate integrated waveguide (SIW) feeding network was used for the first time to feed a patch array. A compensation model was also satisfactory introduced to reduce mutual coupling effects.

In this paper, a linearly polarised patch array fed by a conventional rectangular waveguide (LP-PARW) is presented for the first time. In addition, a complete design as well as a characterisation process model is also specified. A design methodology based on separated antenna modules is followed, with a final integration stage which predicts the full antenna performance. A detailed explanation of the structure is presented in Section 2 and the design process is described in Section 3. Simulated and measured results of the manufactured prototypes to verify the proposed design and characterisation model are detailed in Section 4. Finally, conclusions are drawn in Section 5.

2 Antenna structure description

2.1 Complete antenna structure

The full antenna structure (LP-PARW) is presented in Fig. 1*a*. It consists of two main parts: a rectangular waveguide feeding network (RWFN) and an external double stacked radiating patch array network (RPAN) shown in Figs. 1*b* and *c*, respectively. The RWFN is composed of ICPs (Fig. 1*d*). The travelling wave propagated inside the waveguide is partially coupled by the ICPs and pulled out the waveguide

© The Institution of Engineering and Technology 2014

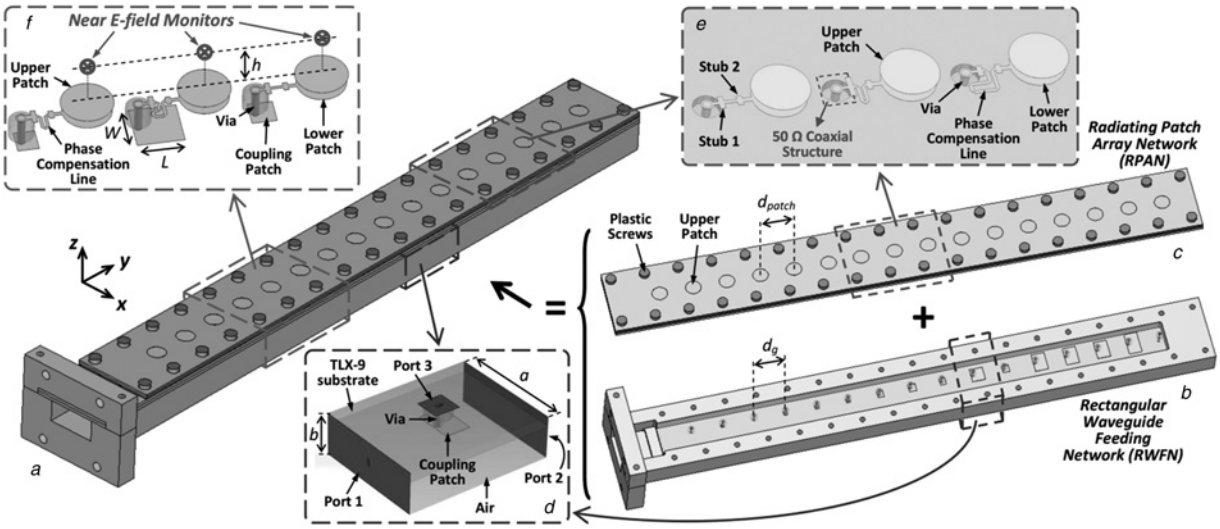

Fig. 1 *Complete antenna structure and separated parts*

a LP-PARW
b Rectangular waveguide feeding network
c Radiating patch array network
d 3-port model ICPs
e Double stacked patches and PCLs topologies
f 3-element mutual coupling model with near E-field monitors

through metallic vias. Therefore each radiating element of the RPAN is connected to its corresponding ICP of the RWFN by these vias. The coupled signal is given to the radiating element (double stacked patch) through a microstrip line (phase compensation line [PCL], Fig. 1*e*) used to tune the radiated phase of each element to achieve broadside radiation. The RPAN is compound by the double stacked patch array and the PCLs which are integrated in the same layer than the lower patch structure.

2.2 Rectangular waveguide feeding network

The RWFN consists of a rectangular waveguide in conventional metallic technology with 16 ICPs inside (Fig. 1*b*). The waveguide width is $a = 18.25$ mm and its height is $b = 6.6$ mm. The travelling wave propagated inside the waveguide is partly coupled to external radiating patches by means of the size (width W and length L in Fig. 1*f*) of these ICPs. Therefore a progressive wave feeding scheme is defined. The size of each ICP is calculated to achieve the desired amplitude feeding distribution. The waveguide is partially filled with a TACONIC TLX-9 substrate (dielectric constant $\varepsilon_{r1} = 2.5$, loss tangent tan $\delta_1 = 0.0019$ and thickness $b_1 = 1.575$ mm) where the ICPs are printed (Fig. 2). Likewise, copper vias of diameter $d_{via} = 1.26$ mm connect the ICPs of the RWFN with the top outside of the waveguide. With this configuration of a partially filled waveguide, the propagated pure TE_{10} fundamental mode is modified into a hybrid Longitudinal Section Magnetic ($LSM^{y'}$) mode [17] providing two different ways of coupling inside the waveguide: the length of the vias and the size of the ICPs. Corresponding to [17], the effective dielectric constant inside the waveguide is $\varepsilon_{reff} = 1.177$ and the cut-off frequency of the fundamental mode ($LSM^{y'}_{10}$) in the equivalent waveguide is 7.58 GHz.

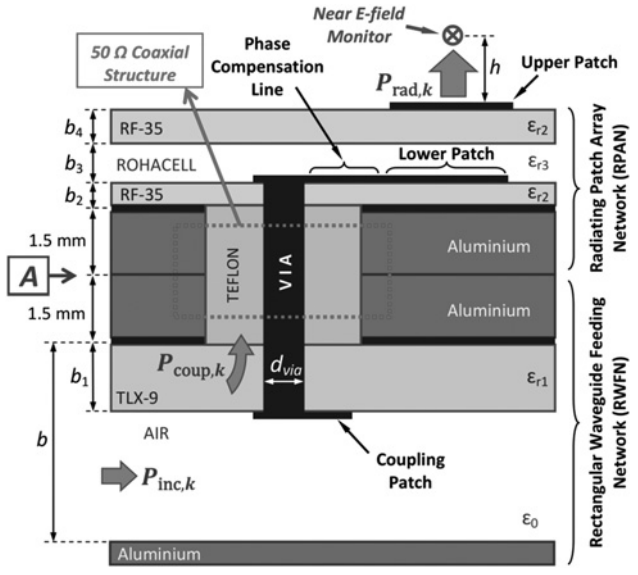

Fig. 2 *Multilayer scheme of the kth element*

2.3 Radiating patch array network

The RPAN is constituted by 16 double stacked circular patches with microstrip PCLs (Fig. 1*c*). As Fig. 2 shows, the stacked patches have been printed on $b_2 = 0.508$ mm (lower patches) and $b_4 = 0.762$ mm (upper patches) TACONIC RF-35 substrates ($\varepsilon_{r2} = 3.5$, tan $\delta_2 = 0.0027$), with a $b_3 = 1$ mm air gap between both layers. The air gap has been implemented using ROHACELL 51 HF ($\varepsilon_{r3} = 1.05$, tan $\delta_3 = 0.004$) substrate to provide mechanical stability to the structure. In addition, the ROHACELL material has been used instead of a higher ε_r material to reduce the surface wave generated between each lower and upper patch layers. Lower patches are directly fed by microstrip PCLs (Fig. 1*e*). The length of each line is adjusted to compensate the phase difference between adjacent radiating elements. This phase difference is because of the distance between elements. The PCLs are

© The Institution of Engineering and Technology 2014

joined with the ICPs of the waveguide by means of metallic vias (d_{via}).

3 Design process

3.1 Proceeding

As preliminary step, the ICPs of the RWFN and the PCLs of the RPAN are separately designed using a basic cell model that only takes into account one single element as designs presented in [7, 12]. Following, both parts individually designed are put together in a full integration antenna evaluating its behaviour. To compensate the mutual effects inside both the waveguide feeding and the radiating structures, a mutual coupling model introduced in [16] between adjacent elements is applied. Finally, a deep comparison of the results before (with the basic cell design) and after the application of the mutual coupling model is presented for evaluating the model performance.

3.2 Rectangular waveguide feeding network

The ICPs are first individually designed in a three port basic cell model (Fig. 1*d*). Input (port 1), output (port 2) and a 50 Ω coaxial structure (port 3) to simulate the impedance of the radiating patch joint are set. The design has been done with the assumption of no losses in the radiating structure ($P_{rad,k} = P_{coup,k}$, with $P_{rad,k}$ and $P_{coup,k}$ the radiated and coupled power of the kth array element in Fig. 2). The amplitude coefficient of each element ($|F_k|$) of a feeding distribution is defined as the radiated power in the element divided by the total array input power

$$|F_k|\ (\text{dB}) = 10 \cdot \log_{10}\left(\frac{|\boldsymbol{E}_k|^2}{\sum_{i=1}^{M}|\boldsymbol{E}_i|^2}\right) \quad (1)$$

$\boldsymbol{E}_k$ is the corresponding field value in the aperture of the kth element of the array and M is the number of elements. For a uniform amplitude feeding distribution, all the amplitude coefficients ($|F_k|$) are equals to −12.04 dB [16]. However, in this work a different amplitude feeding distribution is proposed ($|F_k|_{theo}$ in Table 1) to accomplish a −21 dB side lobe level (SLL) radiation pattern. The coupling coefficients ($|C_k|$ in Table 1) defined as the ratio between the incident ($P_{inc,k}$) and radiated ($P_{rad,k}$) powers in the kth array element are obtained from the coefficients of the proposed amplitude feeding distribution ($|F_k|_{theo}$ in Table 1) by the proceeding shown in [16]. No residual power is considered in the array ($t = 0$ in [16]). Therefore last array element is designed as a matched load to radiate all its incident power. As previously was indicated in Section 2.2, the size of the ICPs defines the antenna feeding distribution. So the required initial ICPs dimensions are directly obtained from the $|S_{3,1}|$ parameter values in the 3-port basic cell model (Fig. 1*d*) to satisfy the calculated $|C_k|$ coefficients in Table 1. No mutual coupling effects between the ICPs are taking into account in this preliminary design process.

Once the sizes of the ICPs have been individually obtained, they are arranged together into the RWFN. The ICPs separation (d_g) has been optimised to achieve the minimum input reflection coefficient of the whole RWFN. In this particular structure, both the element separation (d_{patch}) and the ICPs separation (d_g) are the same ($d_{patch} = d_g$). In [7], a $3\lambda_g/4$ (λ_g is the wavelength of the waveguide) separation between elements was used to cancel the reflections two by two. Nevertheless in this paper, the inclusion of the PCLs adds an extra phase path to its corresponding element. Therefore the reflection coefficient of two adjacent elements k and $k+1$ ($r_{k,\ k+1}$) is redefined in (2) using the singular reflection coefficients of each element (r_k and r_{k+1}), with $|r_k|$, $|r_{k+1}|$, ϕ_k and ϕ_{k+1} the amplitude and phase of the reflection coefficients r_k and r_{k+1}, respectively. β_g is the propagation constant of the waveguide. The amplitude reflection coefficients of adjacent elements ($|r_k|$ and $|r_{k+1}|$) have very similar values. However, their phases (ϕ_k and ϕ_{k+1}) are considerably distinct because of the significant differences between PCLs. For this reason, the initial element separation $d_g = 3\lambda_g/4$ is tuned to achieve the cancellation two by two of the reflection coefficients

$$r_{k,k+1} = |r_k|\ \mathrm{e}^{\mathrm{j}\phi_k} + |r_{k+1}|\mathrm{e}^{\mathrm{j}\phi_{k+1}} \cdot \mathrm{e}^{-2\mathrm{j}\beta_g d_g} \quad (2)$$

Following (2), the distance between elements (d_g) has been optimised obtaining the lowest input reflection with d_g = 18.5 mm ($0.58\lambda_g$) average spacing.

Table 1 LP-PARW amplitude distribution, coupling coefficients and dimensions of ICPs with basic cell and mutual coupling models

Elem.	$\|F_k\|_{theo}$, dB	$\|C_k\|$, dB	Basic cell model		Mutual coupling model	
			L, mm	*W*, mm	*L*, mm	*W*, mm
1	−14.30	−14.30	only via		only via	
2	−14.45	−14.28	only via		1.76	1.76
3	−14.45	−14.12	only via		only via	
4	−12.96	−12.46	1.8	1.76	2.2	1.3
5	−11.80	−11.05	2.37	2.1	2.35	2.5
6	−10.68	−9.57	2.7	3.2	2.2	2.4
7	−10.13	−8.51	3.54	4.1	3.5	4
8	−9.86	−7.59	5.3	5.1	4.3	4.5
9	−9.86	−6.76	6.5	6	3.4	4
10	−10.13	−5.99	7.25	6.95	7.6	7.9
11	−10.68	−5.28	7.65	8.23	4	4.3
12	−11.80	−4.88	7.65	8.9	7.65	10.8
13	−12.96	−4.33	7.65	9.73	7.65	10.5
14	−15.06	−4.43	7.65	9.57	7.65	10.5
15	−15.54	−2.97	7.52	11.82	7.5	12.8
16	−15.63	0	matched load		matched load	

3.3 Radiating patch array network

A 16 element double stacked patch array structure (Fig. 1*c*) has been designed. Each radiating element has been adjusted to 50 Ω. To achieve a broadside radiation, a uniform phase distribution is aimed. The double patch radiating elements are connected to straight microstrip lines placed in the same substrate of the lower patches (Fig. 1*e*). Furthermore, the straight lines are extended and bent to increase their length. These microstrip structures compensate the phase difference between adjacent elements caused by two reasons: the phase factor ($\mathrm{e}^{-\mathrm{j}\beta_g d_g}$) of the progressive wave in the path between two adjacent elements and the phase modification in the transmitted wave under the presence of the ICPs.

Three different topologies of PCLs have been designed (Fig. 1*e*). Bends have been introduced to maintain the location of the whole radiating structure fixed. Thus the diversity of the PCLs does not affect the elements spacing. The longest lines have been doubly bent to shorten the perpendicular microstrip lines for reducing cross-polar (XP)

© The Institution of Engineering and Technology 2014

doi: 10.1049/iet-map.2013.0379

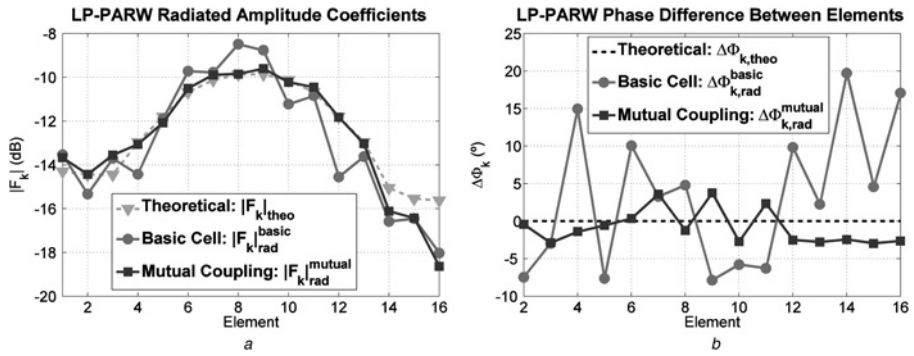

Fig. 3 *LP-PARW theoretical, basic cell and mutual coupling*

a Amplitude coefficients
b Phase difference between elements at 11.5 GHz

radiation and enhancing co-polar (CP) radiation. The impedance of the PCLs is 70 Ω in order to reduce the width; this minimises the undesired radiation of these lines. Furthermore, two microstrip stubs (stub 1 and stub 2 in Fig. 1*e*) have been designed to match the 50 Ω coaxial and the double patch structures to the 70 Ω PCL.

3.4 Mutual coupling compensation model

As it was explained in Section 3.2, the preliminary design of the RWFN was done with the ICPs individually designed in a basic cell model. Besides, in Section 3.3 the lengths of the PCLs were obtained from the individual simulations taking as a reference the previous element [12]. However, mutual effects between adjacent elements degrade the expected radiating behaviour. For this reason, a mutual coupling compensation model presented in [16] has been applied over the integration of the preliminary RWFN and RPAN designs. The model is iteratively applied to the central item of a three element structure whereas the other two act like dummies (Fig. 1*f*). In CST Microwave Studio, the actual radiated amplitude and phase coefficient ($F_{k,\mathrm{rad}}$) of each element is acquired by defining near E-field monitors in the aperture ($h = 1$ mm height above the upper radiating patch) (Figs. 1*f* and 2). Hence, they might be compared with the theoretical ones ($|F_k|_{\mathrm{theo}}$ in Table 1). The phase difference between adjacent elements k and $k-1$ ($\Delta\Phi_k$) is defined in (3)

$$\Delta\Phi_k = \angle F_k - \angle F_{k-1}, \quad \forall k > 1 \tag{3}$$

According to this model, two features have been modified from the initial values of the basic cell model. The size of the ICPs to meet the required amplitude feeding distribution ($|F_k|_{\mathrm{theo}}$ in Table 1), and the length of the PCLs to achieve the desired uniform phase for broadside radiation ($\Delta\Phi_{k,\mathrm{theo}} = 0°$, $\forall k$). In Table 1, a comparison between the size of the ICPs before and after applying the mutual coupling model is shown. Several important changes have been done to the dimensions to accomplish the aimed radiation properties.

The final simulated radiated amplitude coefficients obtained after the mutual coupling model $\left(|F_k|_{\mathrm{rad}}^{\mathrm{mutual}}\right)$ have been greatly adjusted with this method compared with the basic cell design process $\left(|F_k|_{\mathrm{rad}}^{\mathrm{basic}}\right)$ (Fig. 3*a*). The initial phase differences between elements obtained with the basic cell design $\left(\Delta\Phi_{k,\mathrm{rad}}^{\mathrm{basic}}\right)$ have been reduced to less than ±5° with the application of the mutual coupling model $\left(\Delta\Phi_{k,\mathrm{rad}}^{\mathrm{mutual}}\right)$ (Fig. 3*b*).

Moreover, if the RPAN is removed from the integrated structure, the simulated amplitude coupled coefficients form the RWFN (at point A in Fig. 2) obtained after the mutual coupling model $\left(|F_k|_{\mathrm{coup}}^{\mathrm{mutual}}\right)$, suffer critical deterioration compared with the initial basic cell values $\left(|F_k|_{\mathrm{coup}}^{\mathrm{basic}}\right)$ (Fig. 4*a*). This demonstrates that the external mutual coupling effect is much more significant than the internal one because the basic cell results and the theoretical values are practically the same. Therefore the basic cell method is only useful for the initial stage, but then a mutual coupling model over the integrated design is strictly necessary.

To confirm this statement, Fig. 4*b* shows the improvement obtained over the simulations of the radiation pattern after

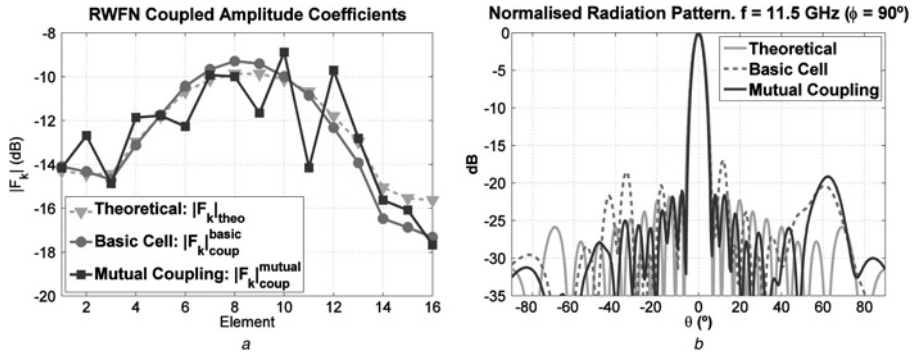

Fig. 4 *Simulation results obtained after applying the mutual coupling model*

a RWFN coupled amplitude coefficients at 11.5 GHz: theoretical, single cell and mutual coupling
b Theoretical and LP-PARW simulated basic cell and mutual coupling normalised radiation patterns at 11.5 GHz ($\phi = 90°$ see axes in Fig. 1)

© The Institution of Engineering and Technology 2014

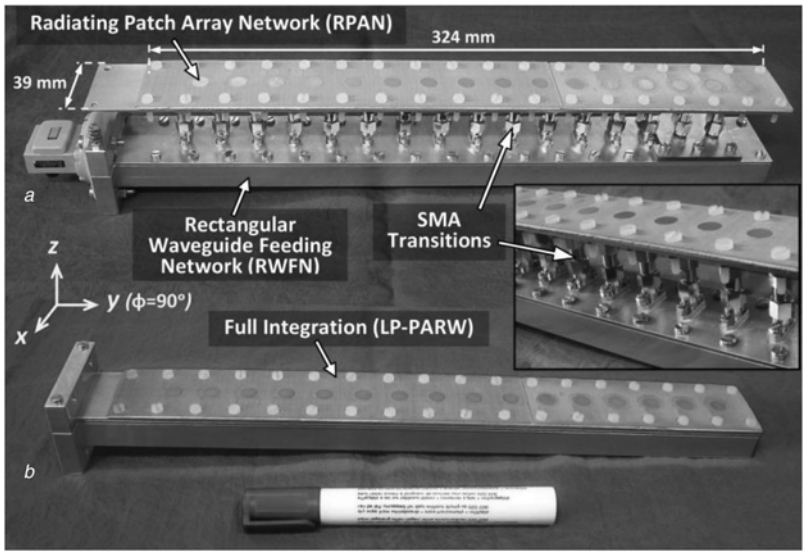

Fig. 5 *Manufactured prototypes*
a RWFN + RPAN
b LP-PARW

applying the mutual coupling model. Practically the whole radiation pattern is adjusted to the theoretical except a misalignment around 60°. This effect can be produced by the spurious radiation of the PCL of each element that is not captured by its corresponding near E-field monitor.

4 Experimental results

RWFN and RPAN connectorised prototypes have been separately manufactured (Fig. 5) and measured. In this case, the metallic vias have been substituted by 50 Ω SMA panel mount connectors for the measurements. The full S-parameters characterisation of both prototypes has been experimentally developed and the complete antenna behaviour has been predicted. Following, both parts are assembled together by 16 SMA male–male transitions (RWFN + RPAN) as is shown in Fig. 5*a* and measured. Finally, a fully integrated prototype of the complete antenna without SMA transitions (LP-PARW) has been also manufactured (Fig. 5*b*) and measured.

A comparative between reflection coefficients of the two manufactured prototypes of the whole antenna (RWFN + RPAN and LP-PARW) is presented in Fig. 6. A notable correlation between simulations and measurements is observed. The interconnection by software of the measured RWFN and RPAN separated S-parameter responses (Meas. RWFN + Meas. RPAN in Fig. 6) have a very similar shape and level than the final measurement of the SMA joint prototype (Meas. RWFN + RPAN in Fig. 6). This demonstrates that the separate design assumption between feeding and radiating networks is possible and predictable with the appropriate mutual coupling model and design process. Even though Fig. 6 shows a certain misalignment between the measured reflections of the full integrated prototype (Meas. LP-PARW in Fig. 6) and the connectorised structure (RWFN + RPAN) because of manufacturing and joint-process tolerances, it is necessary to clarify that the key point of this work is the importance of the mutual coupling model application to realise a correct assumption in the combination of the feeding and radiating structures. In addition, the separated assembly of both components (Fig. 5*a*) corroborates the approximate behaviour of the integrated prototype (Fig. 5*b*). As Fig. 6 shows, the achieved reflection response is under −15 dB in the whole operating band (11–12 GHz).

On the other hand, the RWFN + RPAN and the LP-PARW radiation patterns measured at the $\phi = 90°$ plane (see Fig. 5

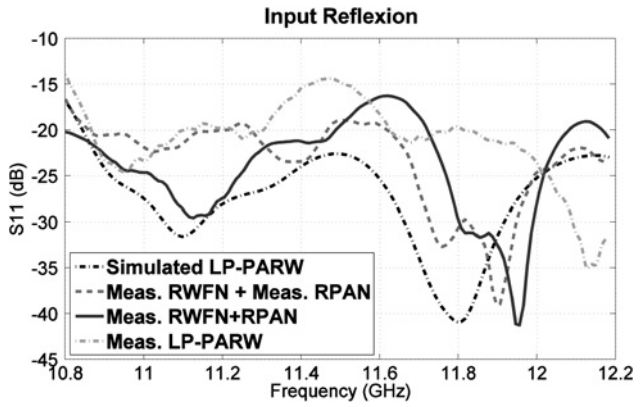

Fig. 6 *Comparison of simulated and measured input reflections*

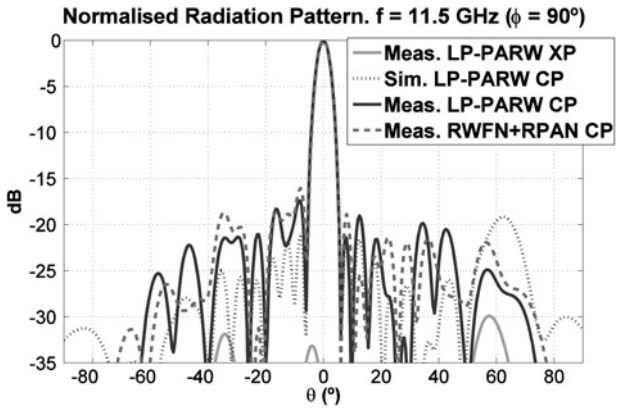

Fig. 7 *Normalised radiation patterns of RWFN + RPAN and LP-PARW prototypes at 11.5 GHz ($\phi = 90°$)*

© The Institution of Engineering and Technology 2014

doi: 10.1049/iet-map.2013.0379

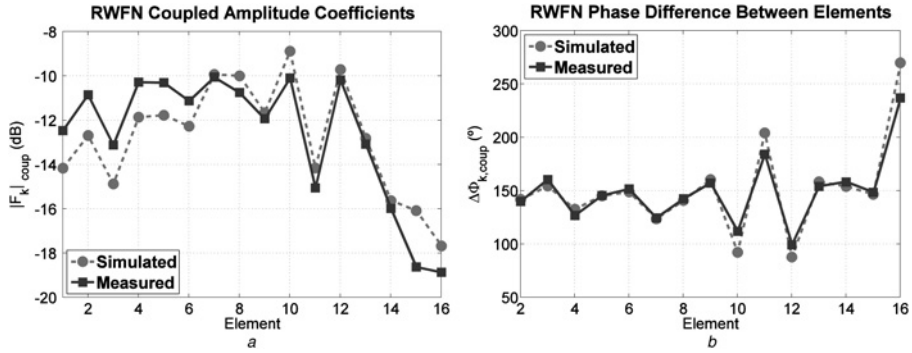

Fig. 8 *Simulated and measured results of RWFN prototype at 11.5 GHz*

a Coupled amplitude coefficients
b Phase difference between elements

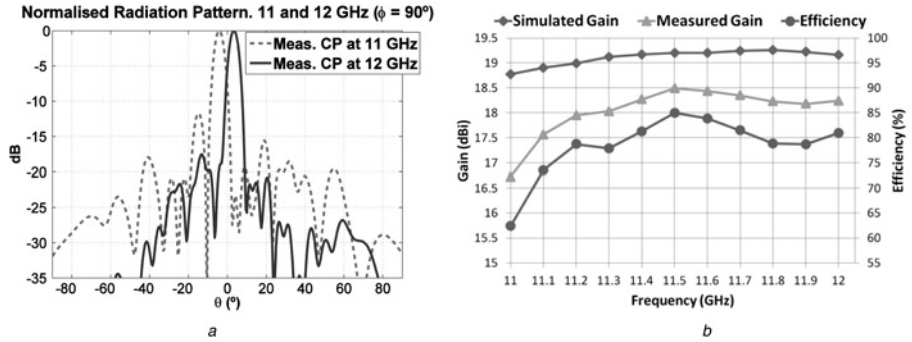

Fig. 9 *Measured and simulated patterns of LP-PARW in frequency band*

a LP-PARW measured radiation pattern at 11 and 12 GHz ($\phi = 90°$)
b LP-PARW gain and efficiency at the main lobe angle: Simulated gain, measured gain and efficiency

axes) are presented in Fig. 7. The broadside radiation observed confirm that the PCLs worked as it was expected. In both cases, a side lobe level below −17.4 dB and a 5° value of −3 dB beamwidth have been obtained at the design frequency (11.5 GHz). A notable level of cross-polar (XP) radiation under −30 dB has also been measured. Nonetheless, a slight asymmetric radiation pattern in the SLL is also observed. The measured $|F_k|_{coup}$ values (at point A in Fig. 2) of the RWFN (showed in Fig. 8*a*) demonstrate that the first six elements couple more power than the expected in the simulations. Likewise, four elements have a small phase deviation from the predicted values (Fig. 8*b*). This deterioration is produced by the tolerance errors during the completely manual manufacturing process. However, the proposed method allows the detection of degradations in each element without the necessity to measure the near radiated field in the aperture of the antenna. According to the observed SLL deviation because of manufacturing tolerances and good polarisation response, this kind of antennas could be suitable for systems with moderate radiation pattern requirements, as high bit rate outdoor mobile communications in X band.

The measured radiation patterns of the LP-PARW ($\phi = 90°$) at different frequencies are shown in Fig. 9*a*. The typical main beam frequency scanning of this kind of progressive wave antennas is verified. Main beam tilt angles at 11 and 12 GHz are −3.5° and 3.5°, respectively. Therefore the usable bandwidth is reduced to 6% (11.15 – 11.85 GHz) under ±2.5° beamtilt criteria [18]. The obtained 6% usable bandwidth is wider in comparison with [18] (3%) and [19] (2.5%). This improvement is because of the lower effective dielectric constant ($\varepsilon_{reff} = 1.177$) in the RWFN which leads to wider bandwidth under the same main beam tilt criteria.

The simulated and measured LP-PARW gain responses, as well as the measured efficiency at the main lobe angle are presented in Fig. 9*b*. The efficiency has been calculated as the ratio between the simulated and the measured gains. Peak gain of 18.5 dBi and 85% efficiency values are obtained at 11.5 GHz. Better efficiency is achieved with this patch array fed by rectangular waveguide design in comparison with previously published papers by authors in SIW [16] (80% at 17 GHz) or parallel plate waveguide [7] (60% at 12 GHz) technologies.

5 Conclusions and future research

In this article, a complete design model for a linearly polarised linear patch array over a rectangular waveguide has been presented. Internal rectangular coupling patches have been used to couple the power inside the waveguide to the radiating elements. External microstrip PCLs have been used to achieve broadside radiation without placement limitation. The proposed methodology considers separated antenna feeding (RWFN) and radiating (RPAN) modules. Likewise, a mutual coupling compensation model has been used for the final adjustments of the full integrated design. The RWFN and the RPAN have been manufactured and measured separately. The final behaviour of the RWFN and the RPAN union (RWFN + RPAN), has been predicted by

© The Institution of Engineering and Technology 2014

their separated characterisation. Finally, a full prototype of the LP-PARW has been also manufactured and measured obtaining a 18.5 dBi gain an 85% efficiency values at the main lobe angles at 11.5 GHz. Also a usable bandwidth of 6% has been achieved. After the analysis of the results, the suitability of the mutual coupling method has been proved.

The following steps in this research are headed towards more flexible systems for compensating the radiated phase as digital, mems or varactor phase shifters. The inclusion of this kind of devices (only possible in the proposed patch structures in the case of rectangular, SIW or parallel plate waveguides feeding topologies) will allow to obtain an adaptive radiation pattern, trending to a smart antenna.

6 Acknowledgment

This work has been supported by the Spanish Government, Ref. TEC2010-17795.

7 References

1 Simmons, A.: 'Circularly polarized slot radiators', *IEEE Trans. Antennas Propag.*, 1957, **5**, pp. 31–36
2 Hirokawa, J., Ando, M., Naohisa, G.: 'Waveguide-fed parallel plate slot array antenna', *IEEE Trans. Antennas Propag.*, 1992, **40**, (2), pp. 218–223
3 Sakakibara, K., Kimura, Y., Akiyama, A., Hirokawa, J., Ando, M., Goto, N.: 'Alternating phase-fed waveguide slot arrays with a single-layer multiple-way power divider', *Proc. Enst. Eng. Microw. Antennas Propag.*, 1997, **144**, (6), pp. 425–430
4 Akiyama, A., Yamamoto, T., Hirokawa, J., Ando, M., Takeda, E., Arai, Y.: 'High gain radial line slot antennas for millimetre wave applications', *IEE Proc. Microw. Antennas Propag.*, 2000, **147**, (2), pp. 134–138
5 Montisci, G., Musa, M., Mazzarella, G.: 'Waveguide slot antennas for circularly polarized radiated field', *IEEE Trans. Antennas Propag.*, 2004, **52**, (2), pp. 619–623
6 Sekretarov, S.S., Vavriv, D.M.: 'A wideband slotted waveguide antenna array for SAR systems', *Progress In Electromagnetics Research M*, 2010, **11**, pp. 165–176
7 Masa-Campos, J.L., Klinger, S., Sierra-Pérez, M.: 'Parallel plate patch antenna with internal rectangular coupling patches and TEN0 mode excitation', *IEEE Trans. Antennas Propag.*, 2009, **57**, (7), pp. 2185–2189
8 Nakano, H., Takeda, H., Kitamura, Y., Mimaki, H., Yamauchi, J.: 'Low-profile helical array antenna fed from a radial waveguide', *IEEE Trans. Antennas Propag.*, 1992, **40**, (3), pp. 279–284
9 Nakano, H., Okuzama, S., Ohishi, K., Mimaki, H., Yamauchi, J.: 'A curl antenna', *IEEE Trans. Antennas Propag.*, 1993, **41**, (11), pp. 1570–575
10 Haneishi, M., Saito, S.: 'Radiation properties of microstrip array antenna fed by radial line'. Antennas Propagation Society Int. Symp. Digest, 1991, pp. 588–591
11 Shavit, R., Pazin, L., Israeli, Y., Sigalov, M., Leviatan, Y.: 'Dual frequency and dual circular polarization microstrip nonresonant array pin-fed from a radial line', *IEEE Trans. Antennas Propag.*, 2005, **53**, (12), pp. 3897–3905
12 Masa-Campos, J.L., Sierra-Pérez, M.: 'Linearly polarized radial line patch antenna with internal rectangular coupling patches', *IEEE Trans. Antennas Propag.*, 2011, **59**, (8), pp. 3049–3052
13 Padilla, P., Muñoz-Acevedo, A., Sierra-Castaner, M., Sierra-Pérez, M.: 'Electronically reconfigurable transmitarray at Ku band for microwave applications', *IEEE Trans. Antennas Propag.*, 2010, **58**, (8), pp. 2571–2579
14 Carrasco, E., Barba, M., Reig, B., Dieppedale, C., Encinar, J.A.: 'Characterization of a reflectarray gathered element with electronic control using ohmic RF MEMS and patches aperture-coupled to a delay line', *IEEE Trans. Antennas Propag.*, 2012, **60**, (9), pp. 4190–4201
15 Weily, A.R., Bird, T.S., Guo, Y.J.: 'A reconfigurable high-gain partially reflecting surface antenna', *IEEE Trans. Antennas Propag.*, 2008, **56**, (11), pp. 3382–3390
16 García-Valverde, D., Masa-Campos, J.L., Sánchez-Olivares, P., Taha-Ahmed, B., Córcoles, J.: 'Linear patch array over substrate integrated waveguide for Ku band', *IEEE Antennas Wirel. Propag. Lett.*, 2013, **12**, pp. 257–260
17 Balanis, C.A.: 'Advanced engineering electromagnetics' (John Wiley & Sons, 1989), pp. 394–414
18 Sanchez Olivares, P., Masa-Campos, J.L., Ruiz-Cruz, J.A., Taha-Ahmed, B.: 'SIW 2D planar array with four cross slots radiator and tuning vias', *Prog. Electromagn. Res. C*, 2013, **40**, pp. 83–92
19 Chen, P., Hong, W., Kuai, Z., Xu, J.: 'A substrate integrated waveguide circularly polarized slot radiator and its linear array', *IEEE Antennas Wirel. Propag. Lett.*, 2009, **8**, pp. 120–123
20 Masa-Campos, J.L., Sierra-Pérez, M.: 'Radial-line planar antenna with microstrip-feed coupling lines', *Microw. Opt. Technol. Lett.*, 2005, **46**, (4), pp. 305–311

© The Institution of Engineering and Technology 2014

doi: 10.1049/iet-map.2013.0379

Copyright of IET Microwaves, Antennas & Propagation is the property of Institution of Engineering & Technology and its content may not be copied or emailed to multiple sites or posted to a listserv without the copyright holder's express written permission. However, users may print, download, or email articles for individual use.